Supporting information (SI)

Interfacial catalytic degradation mechanism of n-hexane over polyhedral Co_3O_4 nanocatalysts derived from topotactic condensation of ZIF-67

Yunlong Guo[a,b], Meicheng Wen[a,b], Guiying Li[a,b], Jiejing Kong[a,b], Shengnan Song[a,b], Qiuxia Liu[a,b], Taicheng An[a,b]*

[a] Guangdong Key Laboratory of Environmental Catalysis and Health Risk Control, Guangdong Engineering Technology Research Center for Photocatalytic Technology Integration and Equipment, Institute of Environmental Health and Pollution control, Guangdong University of Technology, Guangzhou 510006, China;

[b] Guangzhou Key Laboratory of Environmental Catalysis and Pollution Control, Guangdong-Hong Kong-Macao Joint Laboratory for Contaminants Exposure and Health, School of Environmental Science and Engineering, Guangdong University of Technology, Guangzhou 510006, China.

***Corresponding author:** Prof. Taicheng An, E-mail: antc99@gdut.edu.cn.

Chemicals and materials

All chemicals with analytical grade were employed as received without further purification: cobalt nitrate hexahydrate ($Co(NO_3)_2 \cdot 6H_2O$, Aladdin, 98%), commercial Co_3O_4 (com-Co_3O_4, Aladdin, 99%). 2-methylimidazole ($C_4H_6N_2$, Sinopharm, 99%), commercial Pt/Al_2O_3 (com-Pt/Al_2O_3, Sinopharm, 99%), methanol (CH_3OH, Aladdin, 99.5%), ethanol (C_2H_5OH, Aladdin, 99.8%). Ultrapure water (Elga Purelab Classic, 18.2 MΩ. cm) was used through all the experiments.

Catalyst characterization

The properties of samples were characterized by using various techniques. Power X-ray diffraction (XRD) analysis was carried out using an X-ray diffractometer (D8 Advance, Bruker) with Cu Kα radiation (50 kV, 60 mA). Thermogravimetric analysis (TGA) was conducted on a Mettler Toledo apparatus from 30 to 900 °C at a heating rate of 10 $^oC\ min^{-1}$ in air or nitrogen atmospheres. The surface morphologies of the samples were characterized by scanning electron microscopy (SEM) (Su8220, Hitach). The morphologies, element distribution and crystalline state were observed by using transmission electron microscopy (TEM), high-angle annular dark field-scanning transmission electron microscopy (HAADF-STEM) and selected area electron diffraction (SAED), which were operated on a Thermo Talos-F200S microscope (Talos F200S, FEI). The specific surface area, pore size as well as pore volume were investigated on an automatic volumetric sorption analyzer (ASAP2020, Micromeritics). Prior to the measurement, the samples were degassed at 150 °C for 3 h. The surface elements, oxygen species and elemental states of samples were analyzed using X-ray photoelectron spectroscope (XPS) (Escalab 250Xi, Thermo Fisher), in which monochromated Al Kα (1486.6 eV) and C 1s signal at binding energies (BEs) of 284.6 eV were served as an X-ray source and a reference for BEs calibration, respectively. Electron paramagnetic resonance (EPR) was conducted on a Bruker JEOL FA200 spectrometer. Raman characterization was performed on a confocal Raman

Spectroscopy (LabRAM HR Evolution, HORIBA Jobin Yvon), in which the wavelength was fixed to be 532 nm. Hydrogen temperature-programmed reduction (H_2-TPR) experiments were investigated on a chemical adsorption analyzer (MFTP-3060, China). The sample (50 mg) was first pretreated in N_2 flow of 30 mL min^{-1} at 200 °C for 1 h; after cooled to room temperature (RT), the gas was switched to 8% H_2/92% N_2 mixture gas; and then the temperature was increased from RT to 700 °C at a rate of 10 °C min^{-1}, and thus the temperature-signal curve was recorded for analysis.

For the detection of Lewis and Brønsted acid sites on the surface of ZIF-67-derived Co_3O_4 catalysts, pyridine adsorption Fourier transform infrared spectroscopy (Py-IR) was operated by using an FTIR (Tensor 27, Bruker, Germany), of which pyridine was adopted as a probe molecule. First, a certain amount of sample was firstly pressed into a regular wafer and placed into the IR cell connected by a vacuum adsorption apparatus. Then, the sample was pretreated at 250 °C for 2 h under vacuum. After it cooled to room temperature, the spectra were obtained as background. Then, pyridine vapor was introduced until the adsorption saturation. Finally, the Py-IR spectra were obtained at room temperature after the samples were vacuumed at 50, 150, 200, 250 and 300 °C, respectively. The absorption band at 1450 cm^{-1} is used to quantify Lewis acid sites, whereas the quantities of Brønsted acid sites can be calculated from the peak areas centered at 1540 cm^{-1}.[1]

The in situ diffuse reflectance infrared Fourier transform spectroscopy (in situ DRIFTS) experiments were conducted on a Nicolet iS10 spectrometer at a resolution of 4 cm^{-1} with 32 scans, which was equipped with and a diffuse reflectance cell (consisted of two ZnSe windows and one glass observation window) as well as a MCT detector (cooled by liquid nitrogen). First, the catalyst was mixed with KBr at a certain ratio in order to get enhanced intensities of the peaks presented on the spectra, and then the mixed sample was placed on a porous screen located at the bottom of the cell. Afterwards, the sample was pretreated under a N_2 flow of 20 mL min^{-1} at 150 ^oC for 1 h, of which the background spectrum was obtained when the

temperature was reduced to 30 °C. Finally, the mixture gas such as 500 ppm n-hexane/air or 500 ppm n-hexane/N_2 was introduced into the system at a flow rate of 20 mL min^{-1}, and the spectra were measured at different temperatures, which had been automatically subtracted from the background spectrum.

Kinetic studies

For kinetic studies, the turnover frequency (TOF) is demonstrated as molar number of VOCs transformed per active site of catalyst per second, and is performed at certain reaction temperature where VOC conversion is relatively low under a kinetically controlled regime.[2] The kinetic regime means that the reaction rate is not affected by VOC diffusion and only depends on the number of active sites on the catalyst.[3] Hence, the TOF_{Co} relating to the VOC catalytic degradation over ZIFs-derived metal oxide catalysts was calculated according to the following equation:

$$TOF_{Co} = \frac{C\text{VOCs} * X\text{VOCs} * V\text{gas}}{n} \ (s^{-1})$$

where X_{VOCs} (%) represents the VOC conversion. V_{gas} (mol s^{-1}) is the total molar flow rate of VOCs (The molar volume of gas used in the equation is 24.5 L mol^{-1}). C_{VOCs} (%) is the concentration of reactant gas. n (mol) is the molar amount of Co of the catalyst.

For apparent activation energy (E_a) calculation, the overall variation of the mole flow rate and the pressure drop across the reactor are irrespective, and thus the following Arrhenius equation is presented under the assumption of a plug-flow regime and the mass balance.[4]

$$lnY = \ln\left(K_r^0 m_{Cat.}\right) - \frac{E_a}{RT}$$

where

$$Y = \frac{\emptyset_0}{RT_0} ln\left(\frac{y_{in}}{y_{out}}\right)$$

where R is the universal gas constant (8.314 $J \cdot mol^{-1} K^{-1}$, K_r^0 is the reaction constant (mol $Pa^{-1} g^{-1} s^{-1}$), T_0 is the standard temperature (in Kelvin), Φ_0 ($m^3 s^{-1}$) is the total flow rate of VOCs, C_{in} and C_{out} are the VOC concentrations corresponding to the inlet and outlet, respectively, and m (g) is the mass amount of the catalyst. By calculating the above two formulas, the E_a (kJ mol^{-1}) values could be determined.

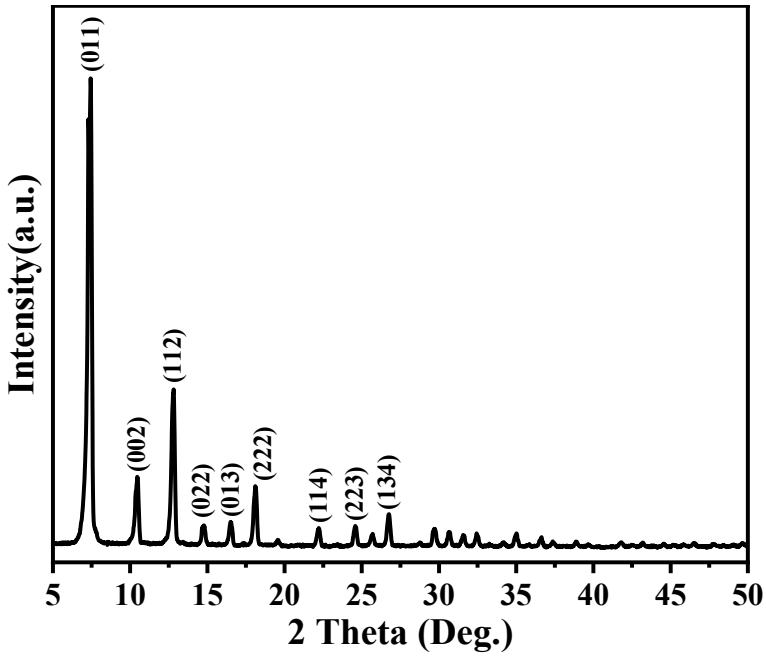

Fig. S1. XRD pattern of original ZIF-67.

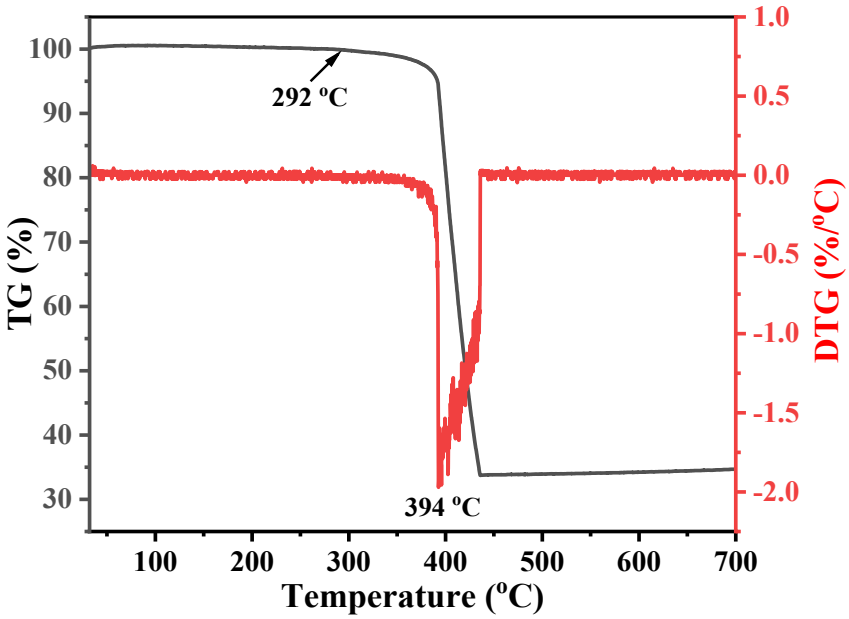

Fig. S2. TGA/DTG curves of original ZIF-67 in air atmosphere.

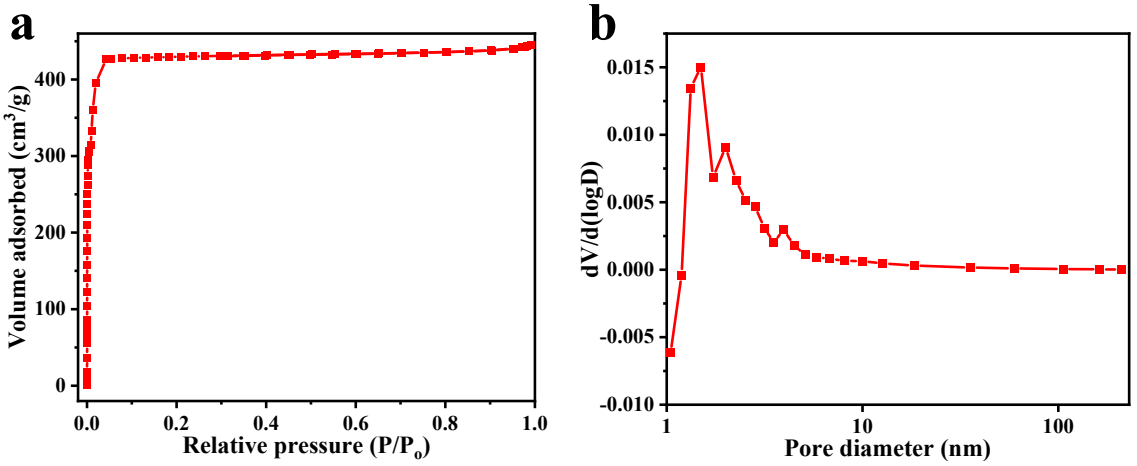

Fig. S3. (a) Nitrogen adsorption-desorption isotherms and (b) the corresponding pore size distributions of ZIF-67 sample.

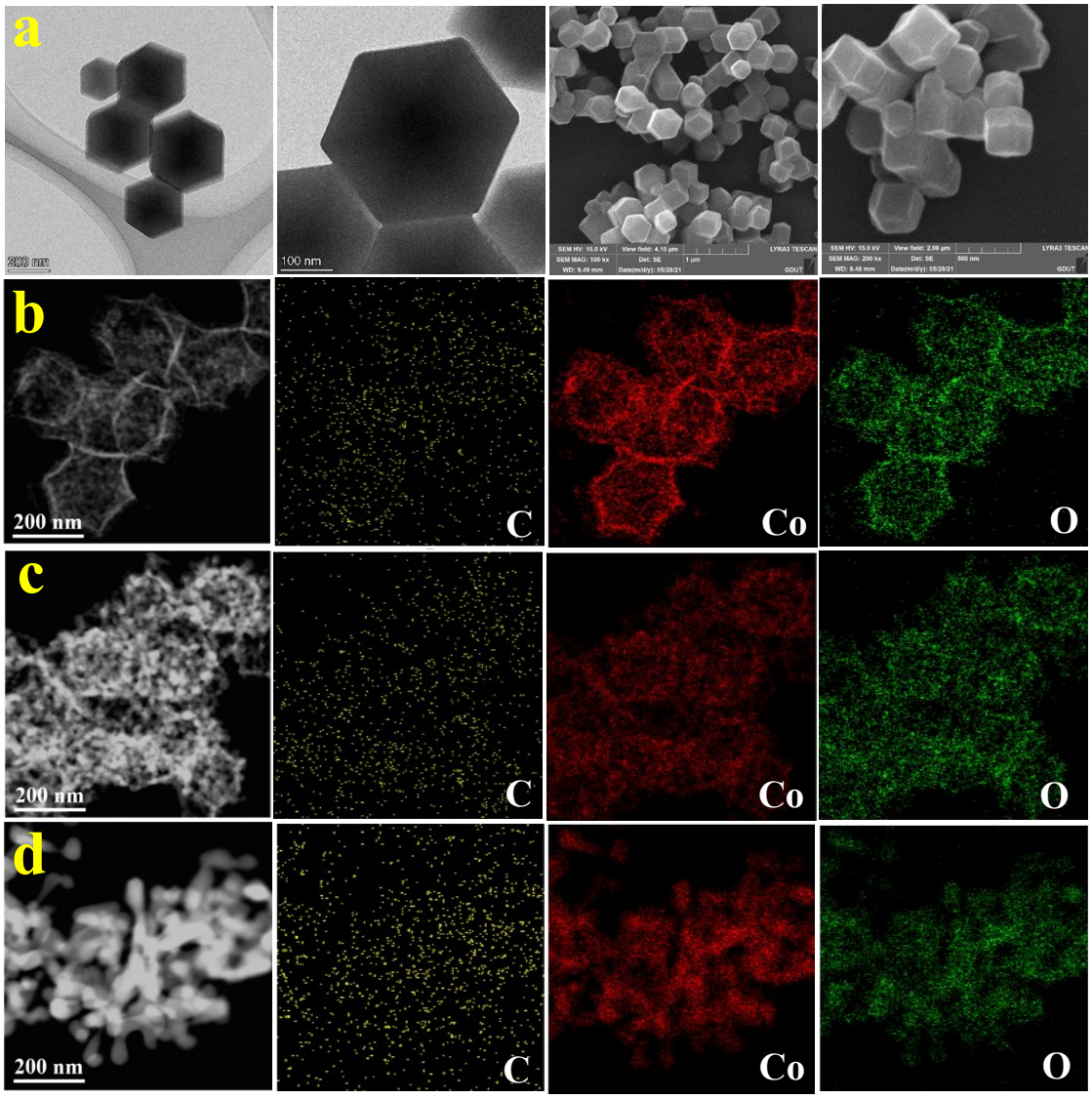

Fig. S4. (a) TEM and SEM images of original ZIF-67. STEM-EDS elemental mapping of (b) Co_3O_4-300, (c) Co_3O_4-400 and (d) Co_3O_4-500.

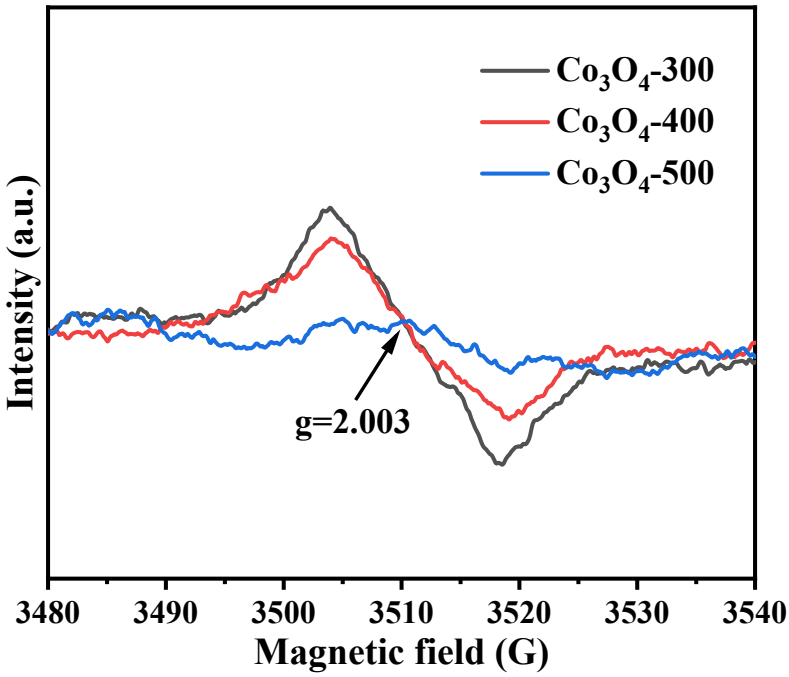

Fig. S5. The EPR spectra of Co_3O_4-300, Co_3O_4-400 and Co_3O_4-500 catalysts.

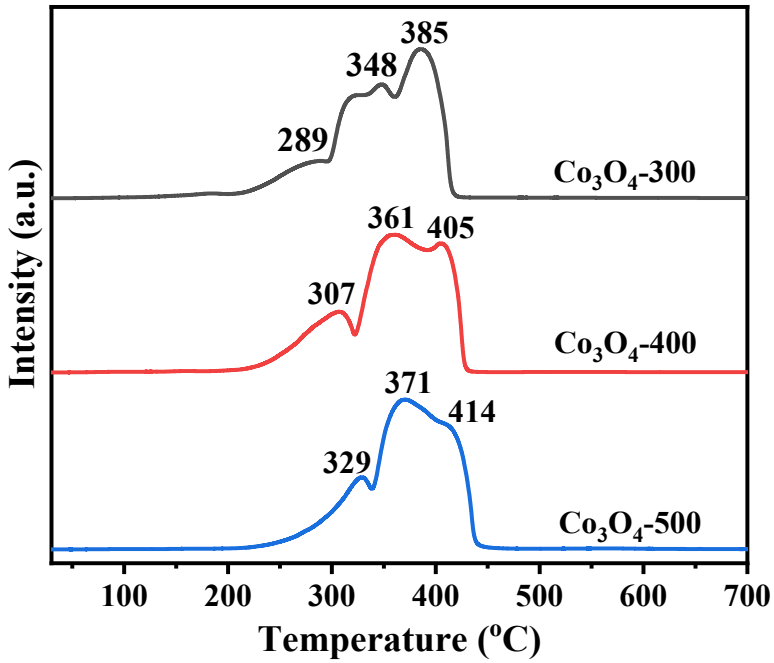

Fig. S6. H_2-TPR profiles of Co_3O_4-300, Co_3O_4-400 and Co_3O_4-500 catalysts.

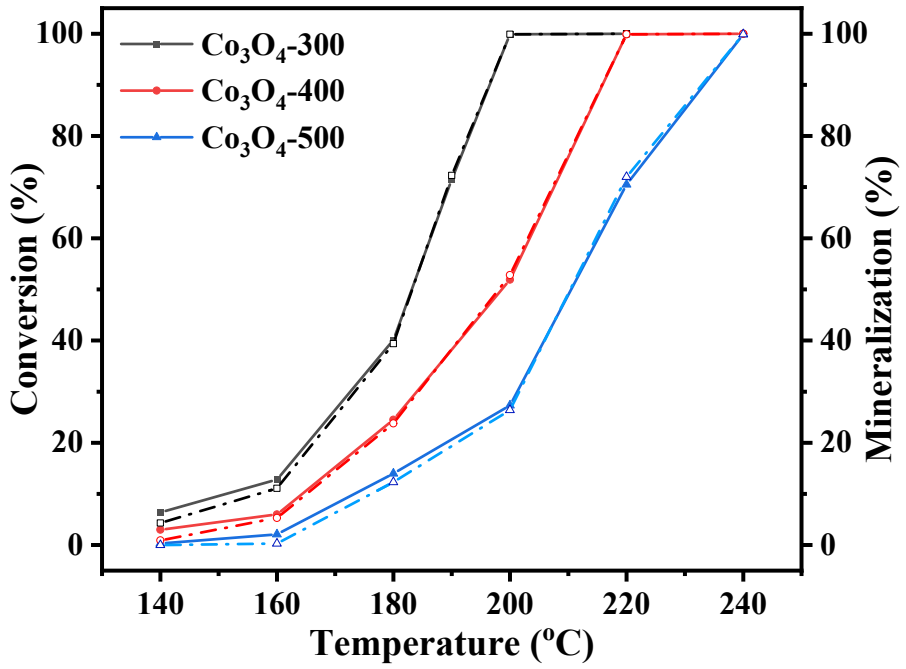

Fig. S7. n-Hexane conversion (solid symbols) and mineralization (dash symbols) as a function of reaction temperature catalyzed by Co_3O_4-300, Co_3O_4-400 and Co_3O_4-500. Note: n-hexane = 500 ppm and GHSV = 60,000 mL g^{-1} h^{-1}.

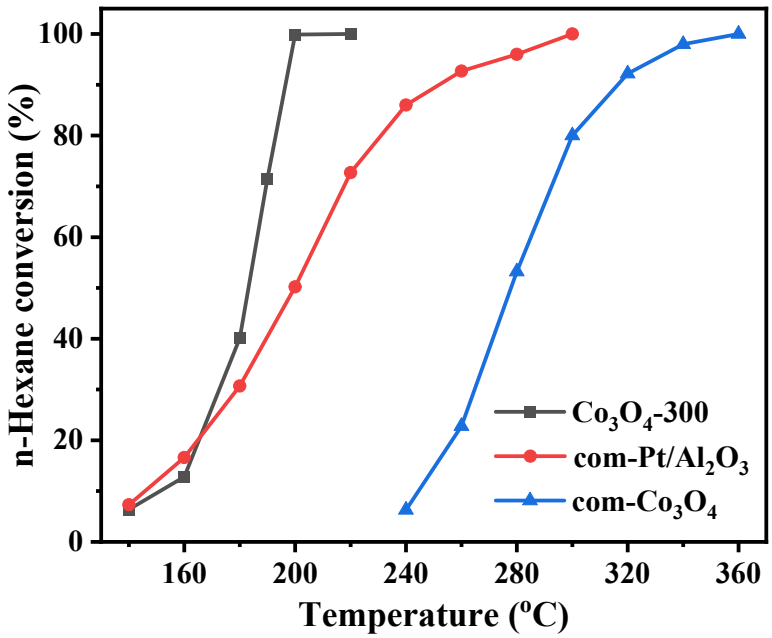

Fig. S8. The conversion of n-hexane as a function of reaction temperature catalyzed by Co_3O_4-300, com-Pt/Al_2O_3 and com-Co_3O_4. Note: n-hexane = 500 ppm and GHSV = 60,000 mL g^{-1} h^{-1}.

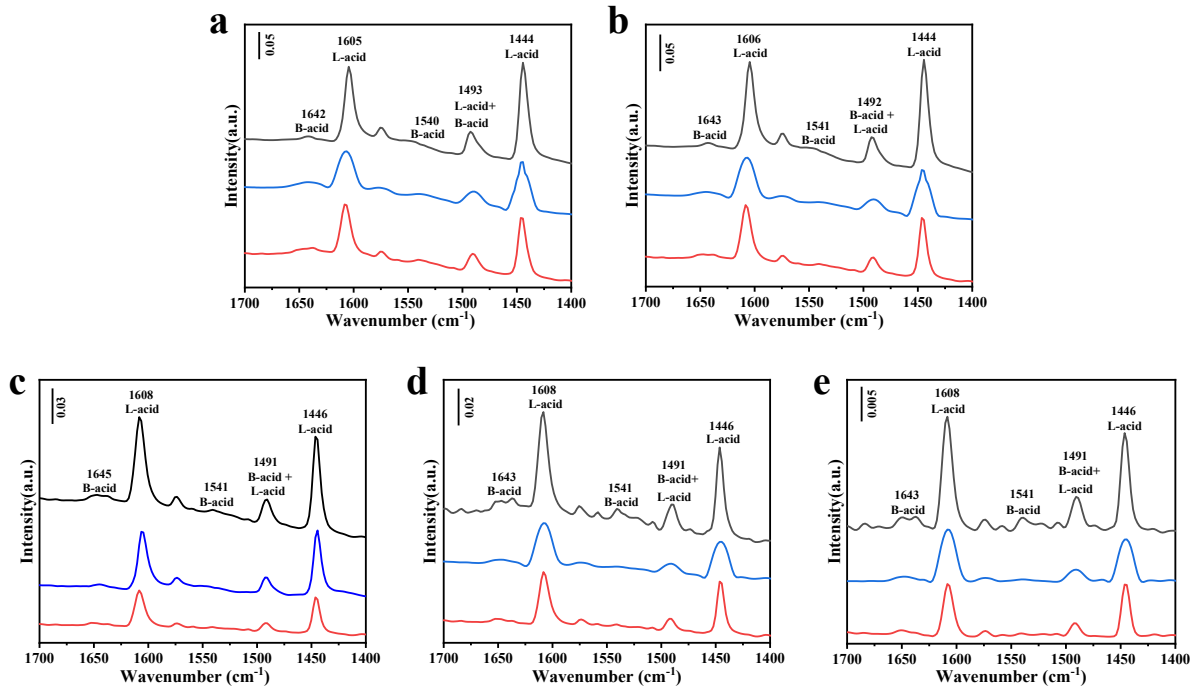

Fig. S9. Py-IR spectra of Co_3O_4-300 (black), Co_3O_4-400 (blue) and Co_3O_4-500 (red) at (a) 50, (b) 150, (c) 200, (d) 250 and (e) 300 °C.

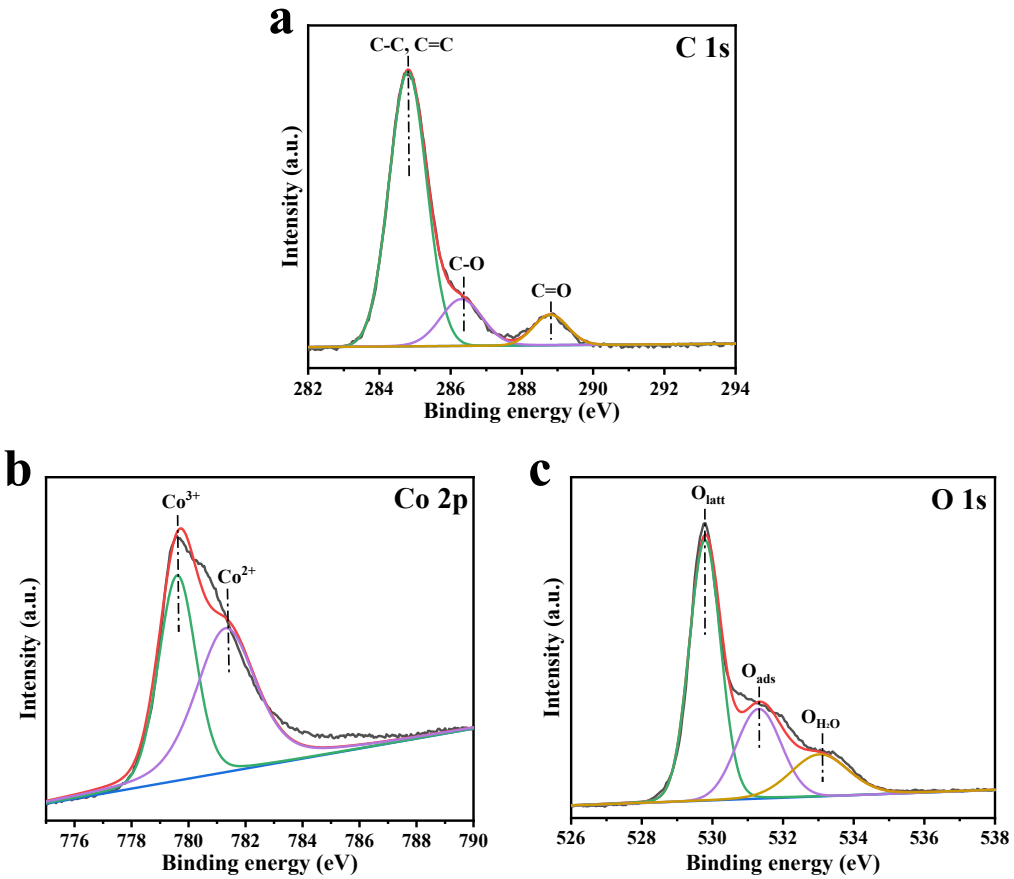

Fig. S10. (a) C 1s, (b) Co 2p and (c) O 1s XPS spectra for Co_3O_4-300 after 90 h of on-stream reaction at different temperatures.

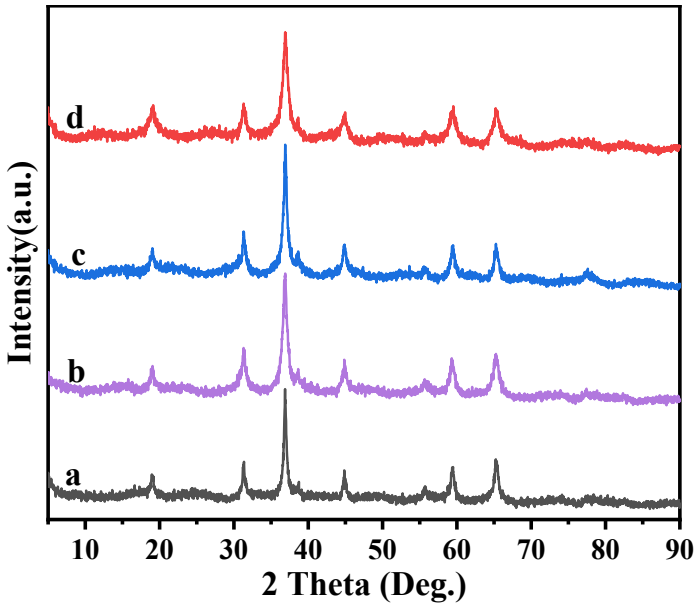

Fig. S11. XRD patterns of Co_3O_4-300 catalyst after reaction of (a) cycle test for 5 times, (b) stability test during 90 h of on-stream reaction, (c) in the presence and absence of 5.0 vol.% water vapor and (d) in the presence and absence of 10.0 vol.% CO_2.

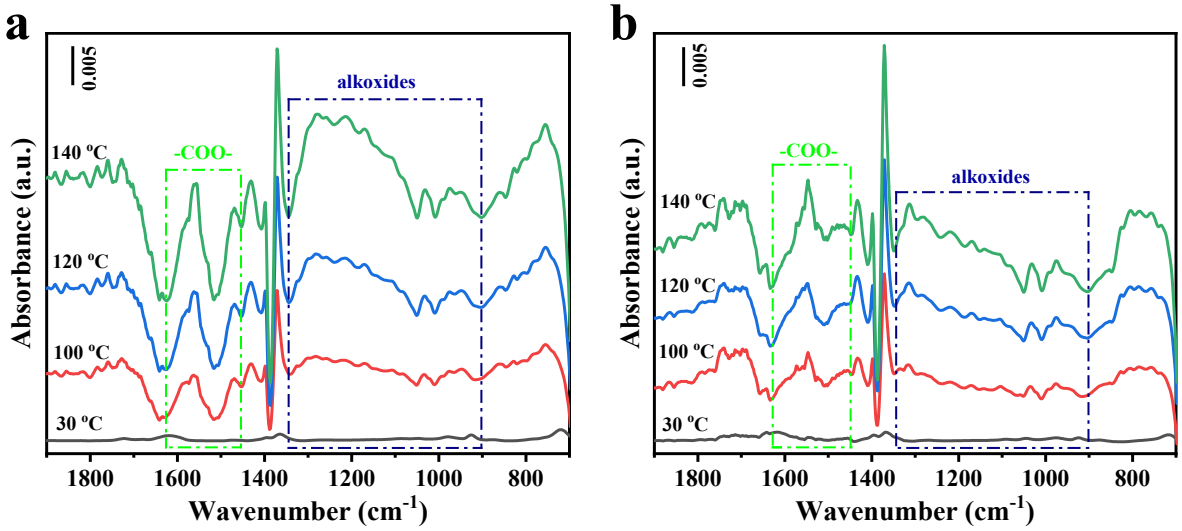

Fig. S12. In situ DRIFTS studies on Co_3O_4-300 at relatively low temperatures under the condition of (a) 500 ppm n-hexane balanced by air and (b) 500 ppm n-hexane balanced by N_2.

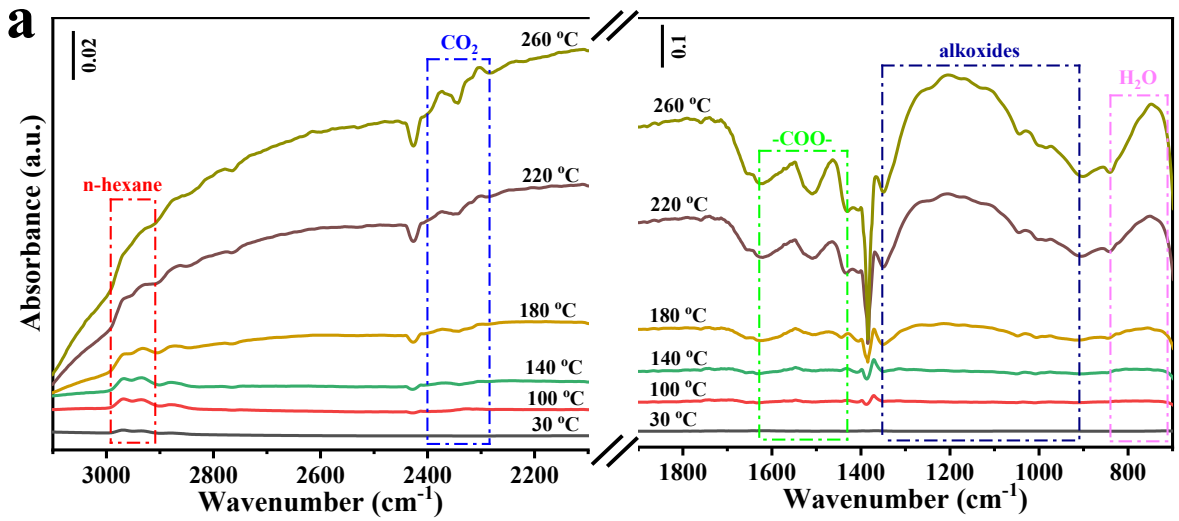

Fig. S13. In situ DRIFTS studies on Co_3O_4-300 under the condition of 500 ppm n-hexane balanced by N_2 at different temperatures.

Table S1 XPS peak area of various C-binding configurations to the total area.

Sample	C 1s		
	C-C, C = C (284.8 eV)	C-O (286.3 eV)	C = O (288.8 eV)
Co_3O_4-300	73.9	14.2	11.9
Co_3O_4-400	78.6	14.7	6.7
Co_3O_4-500	78.7	14.0	7.3
Co_3O_4-300 after 90 h of reaction	77.1	15.1	7.8

Table S2. Catalytic performance of various catalysts toward n-hexane oxidation obtained in this study and reported in the literatures.

Catalyst	Reactant composition	Space velocity (mL g^{-1} h^{-1})	T_{90} (°C)	Reference
0.04Pd SSC/Ti-SBA-15	40 ppm, Air	60,000	310	5
$Ce_{0.97}Cu_{0.03}O_2$	852 ppm, Air	---	350	6
$0.12Pt/Al_2O_3$	1500 ppm, Air	17,500 h^{-1}	400	7
5Co15Mn	2.5 g m^{-3}, Air	14,400 h^{-1}	252	8
CoMn-MS	360 ppm, Air	30,000 h^{-1}	266	9
Co_3O_4-300	**500 ppm, Air**	**20,000**	**187**	**This work**
Co_3O_4-300	**500 ppm, Air**	**60,000**	**196**	**This work**
Co_3O_4-300	**500 ppm, Air**	**100,000**	**199**	**This work**

Table S3 Concentration of acid sites of the three catalysts at various evacuated temperatures.

Sample	Temperature (°C)	$C_{Brønsted}$ (μmol g^{-1})	C_{Lewis} (μmol g^{-1})	C_{total} (μmol g^{-1})	$C_{Lewis}/C_{Brønsted}$
Co_3O_4-300	50	10.6	113.4	124.0	10.7
	150	6.3	92.5	98.8	14.7
	200	3.1	55.0	58.1	17.5
	250	2.3	28.1	30.5	12.1
	300	0.8	9.3	10.2	11.3
Co_3O_4-400	50	9.6	74.1	83.8	7.7
	150	5.0	50.5	55.6	10.0
	200	2.3	44.5	46.8	19.1
	250	0.9	18.0	18.9	19.0
	300	0.3	6.7	7.0	22.8
Co_3O_4-500	50	8.4	61.6	70.0	7.4
	150	4.7	43.5	48.2	9.3
	200	1.1	15.9	16.9	14.9
	250	0.5	13.8	14.3	27.7
	300	0.1	5.5	5.7	38.9

Table S4. The assignment of various species at different peak positions.

Peak position (cm^{-1})	Assignment	Species
2969, 2940	---	n-hexane
2370, 2306	antisymmetric stretching vibration	CO_2
1554, 1467	symmetric or antisymmetric stretching vibration	-COO-
1200	stretching vibrations	alkoxides
749	---	H_2O

References

1 F. Hao, Y. Gao, J. Liu, R. Dudek, L. Neal, S. Wang, P. Liu and F. Li, Zeolite-assisted core-shell redox catalysts for efficient light olefin production via cyclohexane redox oxidative cracking, *Chem. Eng. J.,* 2021, **409**, 128192.

2 X. Wang, L. Yi, T. Zhang, Y. Luo and R. Wang, Geometrical-site-dependent catalytic activity of ordered mesoporous Co-based spinel for benzene oxidation: In situ DRIFTS study coupled with Raman and XAFS spectroscopy, *ACS Catal.*, 2017, **7,** 1626-1636.

3 K. Yang, Y. Liu, J. Deng, X. Zhao, J. Yang, Z. Han, Z. Hou and H. Dai, Three-dimensionally ordered mesoporous iron oxide-supported single-atom platinum: Highly active catalysts for benzene combustion, *Appl. Catal. B: Environ.,* 2019, **244**, 650-659.

4 Z. Rui, S. Wu, C. Peng and H.. Ji, Comparison of TiO_2 Degussa P25 with anatase and rutile crystalline phases for methane combustion, *Chem. Eng. J.,* 2014, **243**, 254-264.

5 M. Wen, S. Song, W. Zhao, Q. Liu, J. Chen, G. Li and T. An, Atomically dispersed Pd sites on Ti-SBA-15 for efficient catalytic combustion of typical gaseous VOCs, *Environ. Sci.: Nano*, 2021, **8**, 3735-3745.

6 V. D. Araújo, M. M. de Lima, A. Cantarero, M. I. B. Bernardi, J. D. A. Bellido, E. M. Assaf, R. Balzer, L. F. D. Probst and H. V. Fajardo, Catalytic oxidation of n-hexane promoted by $Ce_{1-x}Cu_xO_2$ catalysts prepared by one-step polymeric precursor method, *Mater. Chem. Phy.*, 2013, **142**, 677-681.

7 M. Anić, N. Radić, B. Grbić, V. Dondur, L. Damjanović, D. Stoychev and P. Stefanov, Catalytic activity of Pt catalysts promoted by MnO_x for n-hexane oxidation, *Appl. Catal. B: Environ.,* 2011, **107**, 327-332.

8 S. Todorova, H. Kolev, J. P. Holgado, G. Kadinov, C. Bonev, R. Pereñíguez and A. Caballero, Complete n-hexane oxidation over supported Mn–Co catalysts, *Appl. Catal. B: Environ.,* 2010, **94**, 46-54.

9 S. Todorova, A. Naydenov, H. Kolev, J. P. Holgado, G. Ivanov, G. Kadinov and A. Caballero, Mechanism of complete n-hexane oxidation on silica supported cobalt and manganese catalysts, *Appl. Catal. A: Gen.*, 2012, **413-414**, 43-51.